2025 International Conference on Metaverse Computing, Networking and Applications (MetaCom) | 979-8-3315-2255-1/25/$31.00 ©2025 IEEE | DOI: 10.1109/MetaCom65502.2025.00038

Towards a Digital Twin of the Human Kidney for Diagnosis of Renal Diseases

Fenfen Qi
Department of Mathematics
University of Macau
Macau, China

Yingzhi Liu
Department of Mathematics
University of Macau
Macau, China

Yujie Gong
Department of Mathematics
University of Macau
Macau, China

Jing-Yuan Wang
Department of Mathematics
University of Macau
Macau, China

Rongliang Chen
SIAT
Chinese Academy of Sciences
Shenzhen, Guangdong, China

Pengzhi Hu
The Third Xiangya Hospital
Central South University
Changsha, China

Li Luo
Department of Mathematics
University of Macau
Macau, China

Xiao-Chuan Cai
Department of Mathematics
University of Macau
Macau, China

***Abstract*—In this paper, we attempt to develop a digital twin of a human kidney based on patient-specific images, clinically measured data and mathematical models of the kidney tissue, the renal artery, and the renal vein. The aim is to have a sufficiently accurate model so that certain kidney diseases can be analyzed and surgical planning can be carried out virtually and collaboratively on remotely connected mixed reality headsets. To model the hemodynamics of the kidney, we first obtain the patient-specific renal vascular geometry from the CT images and a blood flow model is built with the incompressible Navier-Stokes equations with several patient-specific inflow and outflow conditions. The geometry of the kidney tissue is also obtained from the CT images, and to model the microvascular structure of the kidney with a rich capillary network, we employ the Darcy equations and treat the microvascular bed that cannot be resolved by the CT as a porous medium. For the coupling between the fluid and the porous medium models, we impose three interface conditions based on the conservation of mass, the balance of the normal force and the Beavers-Josepha-Saffman condition. The numerical simulations are implemented offline using a high-end computer cluster and the computational results are rendered online in several holographic headsets, through which doctors can view the hemodynamic details of selected fields collaboratively. Moreover, by connecting and integrating holographic headsets with a high-performance GPU-based workstation, we can compute morphologic and hemodynamic indicators online in real time, aiding in disease diagnosis and treatment planning. Several renal diseases are considered as test cases including renal artery stenosis, renal artery aneurysm as well as localized necrosis of the kidney tissue.**

***Index Terms*—Digital twin, patient-specific kidney, holographic headsets, diagnosis of renal diseases, CFD-based simulation, domain decomposition, parallel computing**

I. Introduction

In the human body, the renal system plays a vital role in maintaining homeostasis by regulating blood pressure, filtering waste, and balancing electrolytes. Renal diseases, such as renal artery stenosis and aneurysm, may lead to the dysfunction of this system that significantly threatens human health. Accurate diagnosis of these diseases is essential but challenging due to the complexity of the renal structure and function. Traditional and non-invasive methods like computed tomography angiography (CTA) are helpful in identifying specific lesion locations. However, these approaches often struggle to precisely quantify hemodynamic information, which is crucial for detecting early-stage pathologies in diseases like chronic kidney disease [1]. Although invasive techniques are available to obtain some hemodynamic data, for instance, the renal fractional flow reserve (FFR) measurements for assessing the risk of renal artery stenosis, they involve complex catheterization procedures that carry potential risks and complications [2], [3]. These limitations highlight a growing need for precise, non-invasive diagnostic tools and personalized treatment strategies to effectively manage renal diseases.

With recent advancements in digital technology, such as holographic visualization, the digital twin has evolved into a powerful tool that can mirror physical objects with virtual representations and dynamically predict their state and behavior through digital simulations. Due to its ability of real-time simulations and precise predictions, the digital twin has been widely applied in different industrial fields [4] such as the machining of aerospace components [5] and the control of autonomous unmanned aerial vehicle landing [6]. There is also a wide range of applications in biomedical engineering [7], [8]. F. Servin et al. [9] introduced a liver digital twin computational model based on the electromagnetic wave equation and the heat transfer equation to simulate microwave ablation therapy and guide clinical decision-making. Gong et al. [10] proposed a digital twin of a human heart to model near-real-time physical deformations by solving hyper-elasticity equations. In [11], the authors developed a digital human brain to visualize anatomical structures and functional areas accurately, and also perform interactive hemodynamic computations for cerebral aneurysms in virtual surgery. By integrating patient-related data with artificial intelligence-based analysis, a patient-specific digital twin can provide individu-

The research is supported by FDCT 0146/2024/RIA2, 0079/2021/AFJ, 0141/2020/A3, 0084/2023/ITP2. F. Qi is the first author and X.-C. Cai is the corresponding author of the paper. Email: xccai@um.edu.mo

979-8-3315-2255-1/25/$31.00 ©2025 IEEE
DOI 10.1109/MetaCom65502.2025.00038

alized clinical decisions for several diseases, such as diabetes [12] and multiple sclerosis [7]. A digital twin model of the renal system utilizing CT-radiography is presented in [13] for the early diagnosis of chronic kidney diseases. However, it is solely based on CT images, capturing morphological features while lacking hemodynamic characteristics needed for a comprehensive understanding and accurate diagnosis of kidney diseases. In this paper, we develop a more realistic digital twin of the human kidney, towards a high-fidelity model that enables intuitive visualization of renal structures and fuses hemodynamic features by a computational model, enhancing diagnostic accuracy. The digital kidney framework comprises an offline simulation of renal blood flows and an online diagnosis of renal diseases.

In the offline phase, our main objective is to compute the high-fidelity hemodynamic results for various disease conditions by numerically simulating the hemodynamics of the kidney based on a coupled multiphysics model. The kidney geometry, including the renal artery, the renal vein and the kidney tissue, is segmented from patient-specific CT images. For the blood flow in the renal vessels, we apply the unsteady incompressible Navier-Stokes equations, while the kidney tissue, treated as a microvascular bed because of the rich capillary network, is modeled by the unsteady Darcy equation. The final multiphysics model consists of these equations with patient-specific boundary conditions and interface conditions [14]. Unlike the previous models on either the vascular system or the organ itself [10], [11], [15], this coupling not only provides the hemodynamic features of blood flows but also accounts for the complex interactions between the vessels and the tissue. This approach has been successfully applied in the simulation of human liver [16], [17] and myocardia [18]. To discretize the model, a finite element method and a second-order time scheme are used, resulting in discretized nonlinear systems. Note that such high-fidelity multiphysics simulations are computationally intensive and highly time-consuming [19]. We employ a Newton-Krylov-Schwarz parallel algorithm on a high-performance computer cluster to numerically solve the discretized systems of the model, thereby reducing the computation time [20]–[22].

In the online phase, the focus shifts to the diagnosis of several renal diseases: renal artery stenosis, characterized by the narrowing of the renal artery that restricts blood flow [23]; renal artery aneurysm, marked by an abnormal bulging of the artery wall that risks rupture [24]; and localized tissue necrosis, identified by the death of kidney tissue due to inadequate blood supply or injury [25]. To enable efficient and collaborative diagnosis of these pathologies, we integrate three key components: interactive visualization of the digital kidney for immersive examination by holographic headsets, real-time computations of hemodynamic indicators by a GPU-based workstation for risk assessments, and a multi-expert collaboration system for synchronized decision-making on the diagnosis. Clinicians equipped with holographic headsets interactively view hemodynamic information from the offline simulation with a particular focus on regions of interest such as stenotic arterial segments, aneurysmal location, or necrotic tissue zones. The connected workstation manages and handles the real-time computations and provides immediate feedback on additional morphologic and hemodynamic indicators, such as degree of stenosis, aspect ratio, renal pressure ratio (RPR), wall shear stress (WSS), flux, and streamlines. The multi-expert collaboration function allows clinicians to share their findings and insights in real time, facilitating a more comprehensive and accurate diagnosis.

The rest of the paper is organized as follows. In Section 2, we introduce the digital twin of a human kidney in detail, including the procedures for offline simulation and online diagnosis of renal diseases. In Section 3, we discuss the applications of the digital twin in understanding and diagnosing three renal diseases: renal artery stenosis, renal artery aneurysm and localized kidney tissue necrosis. Finally, some concluding remarks are presented in Section 4.

II. Framework of digital twin of human kidney

In this section, we introduce a digital twin of the human kidney for the diagnosis of renal diseases. The fundamental framework of the digital twin consists of an offline simulation phase and an online diagnosis phase, as shown in Fig. 1. In the offline phase, the primary task is to conduct numerical simulations of the digital kidney, which specifically involves the following procedures: (a) acquiring clinical kidney imaging data; (b) segmenting and reconstructing the digital kidney geometry including the renal artery, the renal vein and the kidney tissue from image sequences of the renal vessels and the kidney tissue; (c) generating unstructured meshes for the digital kidney; (d) developing a multiphysics mathematical model to describe the blood flows in the digital kidney under the physiological and pathological conditions; (f) performing numerical simulations with efficient numerical methods on a high-end computer cluster. In the online phase, the system facilitates the multi-user collaborative diagnosis of renal diseases through holographic headsets. It includes the remaining processes in Fig. 1: (g) real-time computations of hemodynamic indicators and features in response to users' inputs by a high-performance graphics workstation; (h) collaborative operations and visualizations of the digital kidney and numerical results based on holographic headsets; (e) patient-specific hemodynamic analysis and online diagnosis of certain renal diseases.

A. Offline Simulation of The Digital Kidney

Given the significant computational cost associated with the high-fidelity numerical simulations of blood flows in the digital kidney, we adopt an offline computational strategy within the digital twin framework. In the offline stage, we can simulate different situations of blood flow by adjusting the parameters. In this subsection, we describe a detailed overview of the numerical simulation procedures.

1) Acquisition of clinical data: These clinical kidney imaging data shown in Fig. 1(a), acquired by high-resolution CT scans, were provided by Third Xiangya Hospital of Central

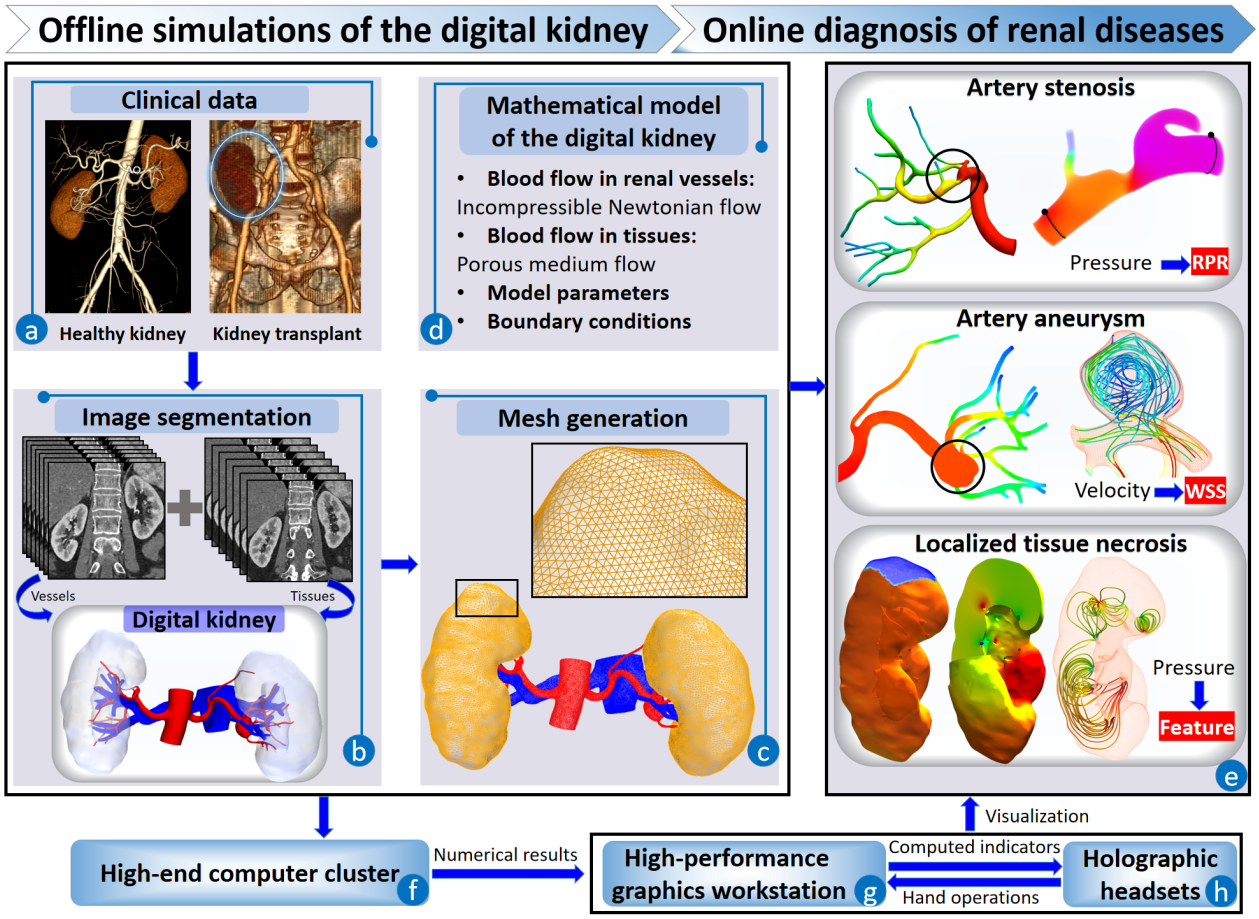

Fig. 1. The basic framework of a digital twin of the human kidney for diagnosis of renal diseases. (1) Offline simulation phase of the digital kidney: (a) some clinical imaging data of the renal vessels and the tissue; (b) a reconstructed 3D digital model of the renal vessels and the kidney tissue segmented from the 2D CT images of the renal vessels and the tissue, respectively; (c) the mesh generation of the digital kidney; (d) the mathematical model of the digital kidney; (f) a high-end computer cluster to perform large-scale hemodynamic calculations in the offline simulation phase. (2) Online diagnosis phase of renal diseases: (g-h) a high-performance graphics workstation and several holographic headsets working together to provide real-time computations and visualization; (e) hemodynamic features and diagnostic indicators for renal diseases such as renal artery stenosis, renal artery aneurysm and localized necrosis of the kidney tissue.

South University (Changsha, China), under institutional review board approval with de-identification ensured in accordance with ethical standards. In addition, there are also some common clinical hemodynamic data including the systolic and diastolic pressures and pulsatile velocity in the renal artery, measured by the sphygmomanometer and the Doppler ultrasound, respectively.

2) Image segmentation and reconstruction: To reconstruct the 3D geometries, the CT image sequences of the renal vessels and the kidney tissue are imported into Mimics, respectively, and then we choose threshold-based and region-growth methods with proper manual labels to segment and extract the regions of interest. Some post-processing techniques like smoothing methods are typically required to obtain the regular 3D kidney geometry shown in Fig. 2(d), where the renal artery, the renal vein and the kidney tissue are labeled in red, blue and transparent yellow, respectively.

3) Mesh generation and partition: For the numerical simulation, we generate an unstructured tetrahedral mesh for the 3D kidney geometry, ensuring that the mesh is matched on the interface between the renal vessels and the kidney tissue. Due to the multiscale structure of the geometry, the different mesh sizes are used in different parts to balance computational efficiency and resolution accuracy. Moreover, the mesh is partitioned some non-overlapping subdomains for the purpose of parallel processing, which can be obtained by METIS or ParMETIS. An example with 12 subdomains is shown in Fig. 3, with each subdomain highlighted with different colors.

4) Mathematical model of the digital kidney: To simulate the blood flow in the digital kidney, denoted as Ω, a multi-physics model is considered that couples the blood dynamics in the renal vessels (free-flow region) Ω_f with the blood

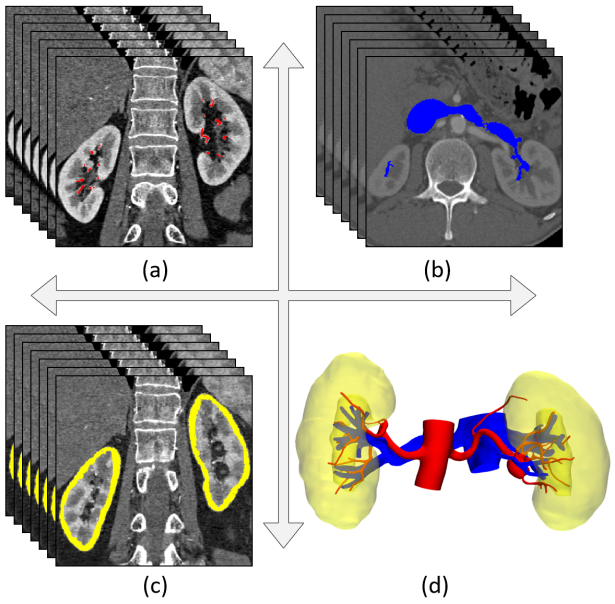

Fig. 2. (a) 2D CT images of the renal artery marked in red. (b) 2D CT images of the renal vein marked in blue. (c) 2D CT images of the kidney tissue marked in yellow. (d) Reconstructed 3D renal artery, the renal vein and the kidney tissue colored in red, blue and yellow, respectively.

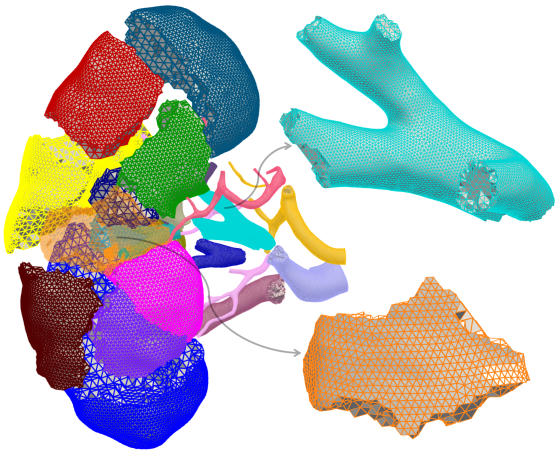

Fig. 3. A non-overlapping domain decomposition of the digital kidney for the numerical computation in parallel.

dynamics in the kidney tissue (porous medium region) Ω_p. Specifically, in the free-flow region Ω_f, we introduce the unsteady incompressible Navier-Stokes equations

$$\begin{cases} \rho\left(\frac{\partial \boldsymbol{u}_f}{\partial t} + (\boldsymbol{u}_f \cdot \nabla)\boldsymbol{u}_f\right) - \nabla \cdot \mathbb{T}(\boldsymbol{u}_f, p_f) = 0, \\ \nabla \cdot \boldsymbol{u}_f = 0, \end{cases} \tag{II.1}$$

where $\boldsymbol{u}_f$ and p_f are the blood velocity and pressure in the vessels, respectively, $\mathbb{T}(\boldsymbol{u}_f, p_f) = 2\mu\mathbb{D}(\boldsymbol{u}_f) - p_f\mathbb{I}$ is the Cauchy stress tensor, $\mathbb{D}(\boldsymbol{u}_f) = \frac{1}{2}(\nabla \boldsymbol{u}_f + \nabla^T \boldsymbol{u}_f)$ is the strain rate tensor and $\mathbb{I}$ is the identity tensor, ρ is the blood density

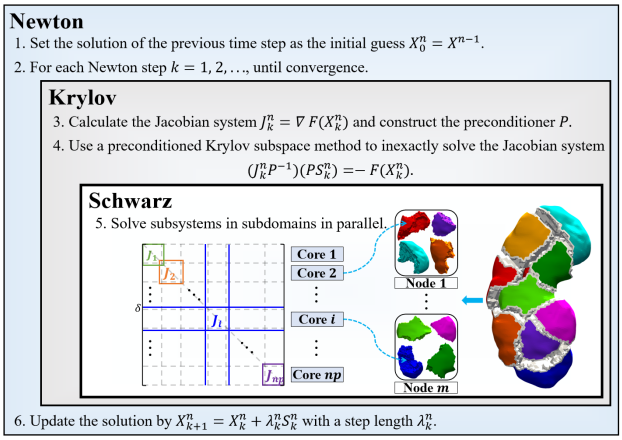

Fig. 4. The framework of the Newton-Krylov-Schwarz parallel algorithm.

and μ is the kinematic viscosity of the blood. For the blood flow in the porous medium region Ω_p, it is governed by the Darcy equation

$$S_0 \frac{\partial p_p}{\partial t} - \nabla \cdot (\mathbb{K}\nabla p_p) = 0, \tag{II.2}$$

where p_p is the pressure in the porous medium domain, S_0 denotes the mass storativity coefficient and $\mathbb{K}$ represents the permeability tensor. The models (II.1) and (II.2) are coupled by the following three conditions on the interface Γ

$$\begin{aligned} &\boldsymbol{u}_f \cdot \boldsymbol{n} + (\mathbb{K}\nabla p_p) \cdot \boldsymbol{n} = 0, \\ &-\boldsymbol{n} \cdot (\mathbb{T}(\boldsymbol{u}_f, p_f) \cdot \boldsymbol{n}) = p_p, \\ &-\boldsymbol{\tau}_i \cdot (\mathbb{T}(\boldsymbol{u}_f, p_f) \cdot \boldsymbol{n}) = \alpha \boldsymbol{\tau}_i \cdot \boldsymbol{u}_f, \ (i = 1, 2), \end{aligned}$$

where $\boldsymbol{n}$ denotes the unit outward normal vectors to the free flow region, $\boldsymbol{\tau}_i$ denotes the unit tangential vectors to the interface and α is a parameter. For the well-posedness of the multiphysics model, initial and boundary conditions must be specified. The initial conditions are given by

$$\boldsymbol{u}_f(\boldsymbol{x}, 0) = \boldsymbol{u}_0(\boldsymbol{x}), \quad p_p(\boldsymbol{x}, 0) = p_{p,0}(\boldsymbol{x}),$$

where $\boldsymbol{u}_0$ is the initial velocity and $p_{p,0}$ is the initial pressure. On the boundaries, we impose the following conditions

$$\begin{aligned} \boldsymbol{u}_f &= \boldsymbol{u}_I, \quad \text{on } \Gamma_I \\ \boldsymbol{u}_f &= \boldsymbol{0}, \quad \text{on } \Gamma_f \\ -\mathbb{T}(\boldsymbol{u}_f, p_f) \cdot \boldsymbol{n} &= p_O \cdot \boldsymbol{n}, \quad \text{on } \Gamma_O, \\ \mathbb{K}\nabla p_p \cdot \boldsymbol{n} &= 0, \quad \text{on } \Gamma_p, \end{aligned}$$

where $\Gamma_I, \Gamma_O, \Gamma_f$ and Γ_p represent the inlet of the artery, the outlet of the vein, the wall of the vessels and the wall of the kidney, respectively, $\boldsymbol{u}_I$ is the inlet velocity and p_O is the outlet pressure.

5) Numerical discretization and offline parallel algorithm: To numerically solve the continuous multiphysics problem, we use a finite element method and a backward differentiation formula to discretize the problem and form a nonlinear system

$$F^n(X^n) = 0, \tag{II.3}$$

at each time step t^n, where X^n is a vector representing the values of numerical velocity and pressure at mesh points. Then, a Newton-Krylov-Schwarz (NKS) parallel algorithm [26] is utilized to solve the system (II.3), see Fig. 4, in which we typically perform the main steps to find the solution at each time step, as follows.

Step 1: Let X_0^n be the initial guess. A Newton method is employed as the nonlinear solver, and at each Newton step, the linear Jacobian system is solved inexactly with a preconditioned Krylov subspace method

$$J_k^n s_k^n = -F^n(X_k^n)$$

to determine the Newton direction s_k^n.

Step 2: Update the iterative approximate solution by

$$X_{k+1}^n = X_k^n + \lambda_k^n s_k^n,$$

where λ_k^n is a step size satisfying the Armijo-Goldstein condition [27]. If the residual $F^n(X_{k+1}^n)$ reaches the prescribed threshold tolerance, we terminate the iteration and set it as the current iterative approximate solution X^n.

For the parallel computation in the numerical simulations, each processor is assigned a subdomain $\Omega_i, i = 1, \ldots, np$, and handles the computation related to the subdomain. In NKS method, the additive Schwarz preconditioner is also constructed by these subdomains, and takes the form

$$P^{-1} = \sum_{i=1}^{np} (R_i^0)^T J_i^{-1} R_i + R_0^T J_0^{-1} R_0,$$

where R_i^0 and R_i in the first term are matrices that restrict the global data to the corresponding local data in each non-overlapping and each overlapping subdomain, respectively, J_i is the subdomain Jacobian matrix for $i = 1, \ldots, np$. The second term is intended to improve the scalability of the parallel algorithm and its construction is based on a suitable coarse problem [21], [28], [29].

B. Online Diagnosis for Renal Diseases

Following the offline simulation, the high-fidelity numerical results are now available for real-time holographic analysis and online diagnosis. In this subsection, we describe the online procedures within the digital twin, encompassing the holographic visualization, the real-time interactive computation and the collaborative diagnosis.

1) Holographic visualization of the digital kidney: The numerical results are loaded into the online system which features several holographic headsets and a powerful GPU-based workstation. The holographic headsets are responsible for presenting such as the holographic kidney and the color rendering of numerical results, while the workstation manages the real-time visualization computations to accommodate changes in position and orientation controlled by hand gestures, as shown in Fig 5. By means of the online system, visualizations of the 3D digital kidney and the numerical results can be achieved, allowing us to have a more immersive interaction and deeper understanding of the kidney.

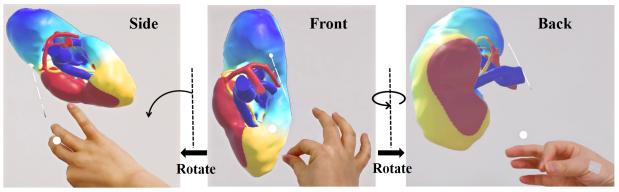

Fig. 5. Visualization of the digital kidney with numerical results from different perspectives using hand gestures, where color gradients represent the pressure distribution.

2) Real-time indicator computations for quantitative assessment: To quantify the risk of renal diseases, the online system also provides the real-time generation of streamlines and computations of risk indicators such as flux, RPR and WSS. These computations, based on the numerical results from the offline simulation, are processed rapidly with minimal latency using the high-performance GPU-based workstation. The blood flux at a cross section S is defined by

$$\text{flux} = \int_S \boldsymbol{u} \cdot \boldsymbol{n} dS, \tag{II.4}$$

which is approximately computed by a numerical integration in a triangulation of the cross section. The triangulation of a cross section can be obtained by the intersection between the cross section and the 3D kidney mesh. The RPR is calculated as a ratio

$$\text{RPR} = \frac{\bar{p}_d}{\bar{p}_a}, \tag{II.5}$$

where $\bar{p}_d$ and $\bar{p}_a$ are the average pressures at the proximal and the distal cross sections of the stenosis, respectively. These cross sections can be chosen by the online system and the calculation of the average pressures is similar to that of the blood flux. For the renal aneurysm, we compute the WSS [30] and the average WSS (AWSS) by

$$\text{WSS} = \mu |\nabla \boldsymbol{u} \cdot \boldsymbol{n} - ((\nabla \boldsymbol{u} \cdot \boldsymbol{n}) \cdot \boldsymbol{n}) \boldsymbol{n}|, \tag{II.6}$$

and

$$\text{AWSS} = \int_{S_{an}} |WSS| dS_{an}, \tag{II.7}$$

in the aneurysm wall region S_{an}, respectively, shown in Fig. 6. The streamlines $\boldsymbol{x}(s)$, satisfying the ordinary differential equations

$$\frac{d\boldsymbol{x}}{ds} = \boldsymbol{u}(\boldsymbol{x}), \tag{II.8}$$

can be approximated by a numerical integration using the fourth-order Runge-Kutta method, starting from initial seed points; see Fig. 7. In this case, the velocity field $\boldsymbol{u}$ is provided directly in the renal vessels and computed in the kidney tissue using Darcy's law $\boldsymbol{u} = -\mathbb{K} \nabla p_p$. In addition, it is also available to measure the morphologic parameters such as the aspect ratio of aneurysm and degree of stenosis by the distance; see Fig. 6(b). These computations are seamlessly interactive and real-time in the online system by user-defined operations in holographic headsets and function-based processing in the GPU-based workstation.

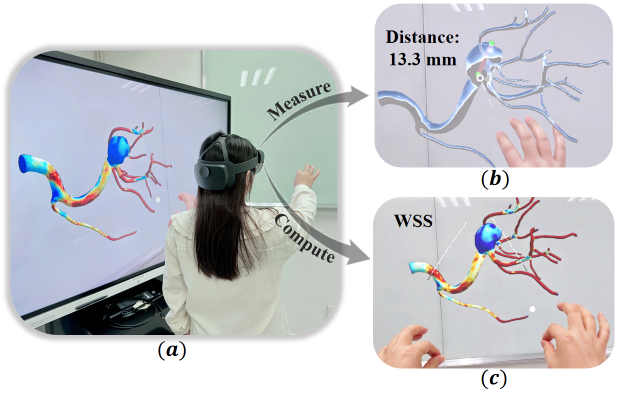

Fig. 6. Real-time computation of morphologic and hemodynamic indicators. (a) Holographic-based interaction through hand operations; (b) distance measurement by moving the positions of initial two points; (c) computation and visualization of the wall shear stress.

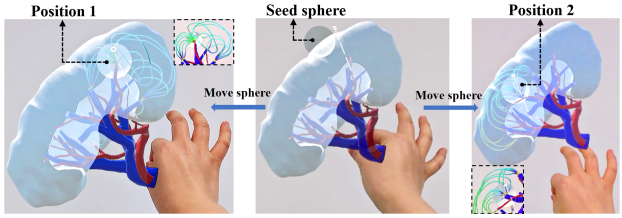

Fig. 7. Real-time computation of local streamlines by adjusting the position of the initial seed sphere.

3) Multi-expert collaborative diagnosis: The collaborative diagnosis technique is realized in the way of the host's operation and client participation [15]. The session host can manually label areas of interest and add comments via speech recognition, guiding collaborators to these labeled locations. All experts can share the real-time computational streamlines and indicators. For instance, for the streamline computation and share, the host provides a sphere's information including the center and radius for the generation of seed points and additional options. After receiving the post-processing command from the host, the GPU-based workstation then fulfills the computation in real time. Each expert has access to the same results, which can be viewed independently by themselves. In the process of data sharing, only a small amount of data needs to be exchanged, allowing collaboration to be completed in real time.

III. Results and Discussion

In this section, we discuss the applications of the proposed digital twin of the human kidney in certain renal diseases including renal artery stenosis and renal artery aneurysm as well as localized kidney tissue necrosis, enabling medical experts to collaboratively diagnose these diseases online in real time. The digital kidney also has the potential to help us understand the physiological interactions between the renal vessels and the kidney tissue, to be precise, how the kidney tissue responds to renal vascular diseases and how renal vessels react to the kidney tissue conditions.

A. Case study I: Renal artery stenosis

Renal artery stenosis may lead to a reduced blood supply for the downstream tissues and organs, which depends on the severity of the stenosis. In contrast to conventional diagnostic methods limited to anatomical features and invasive devices, the proposed digital kidney can non-invasively provide both morphological and hemodynamic information, such as the degree of stenosis and the RPR, a significant indicator for assessing the impact of a stenosis on blood flow. Especially in the case of coronary artery stenosis, it is referred to as FFR, a gold standard with a critical threshold of 0.8 [31]. Using the proposed digital twin, a doctor can view the digital kidney in detail such as the pressure distribution and risk indicators shown in Fig. 8 by an interactive interface and share them with other doctors in different places for real-time collaborative diagnosis. As shown in Fig. 8(a), the pressure reaches 125 mmHg at the main renal artery and drops gradually to 22 mmHg at the outlet. For the morphologic diagnosis, users can quickly locate the stenotic segment and measure the diameter and area of the stenotic section, and then use them to quantify the degree of stenosis (66.7% diameter stenosis shown in Fig. 8(b)). To further investigate the hemodynamic significance of the stenosis, users can compute the RPR in real time by choosing the proximal and distal cross sections that are 6 mm away from the stenotic segment to calculate the average pressures. In Fig. 8(c), we show the distribution of the pressure on the two cross sections and the average pressures are 120 mmHg proximally and 99 mmHg distally, respectively. The computed RPR value of 0.83 suggests a 17% reduction in blood flow to the downstream vessels. For an optimal treatment plan, the digital twin enables multi-expert collaboration online by integrating the anatomical location, severity and hemodynamic impact of the stenosis.

B. Case study II: Renal artery aneurysm

Unlike renal artery stenosis, while the renal artery aneurysm is a rare renal disease with an overall incidence of 0.09% within the general population, it carries the risks of growth and rupture [32]. For the accurate risk assessment of an aneurysm, the proposed digital kidney offers interactive computations of the aspect ratio, a morphological parameter defined as the ratio of the aneurysm height (h) to the neck width (d), and the AWSS hemodynamic indicator reflecting the effect of blood flow on the aneurysm wall. In Fig. 9, we show the computational results of a renal artery aneurysm case. In this case, the aspect ratio is 1.52 slightly below the high-risk threshold of 1.6 introduced in [33] for cerebral aneurysms and the AWSS is 2.07 Pa associated with the aneurysmal rupture [34]. Moreover, details of the flow pattern in the aneurysm, such as the complex streamlines describing the vortex structures, can also be observed. These important indicators and hemodynamic features provided by the digital twin are useful

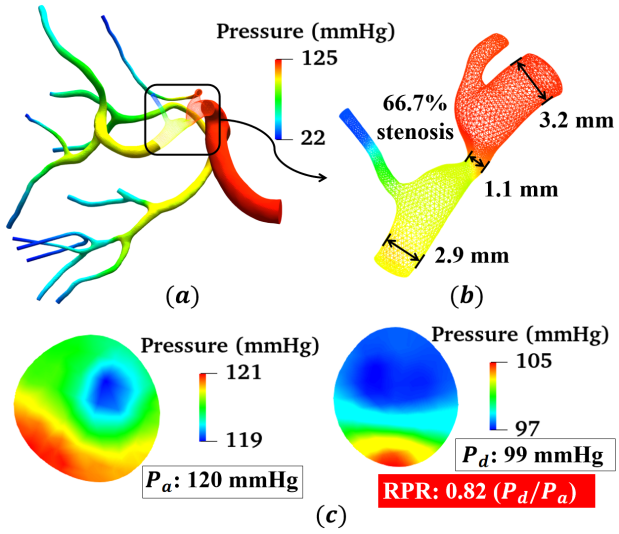

Fig. 8. Renal artery stenosis case: the pressure distribution (a), the morphologic degree of stenosis (b) and the hemodynamic renal pressure ratio (c).

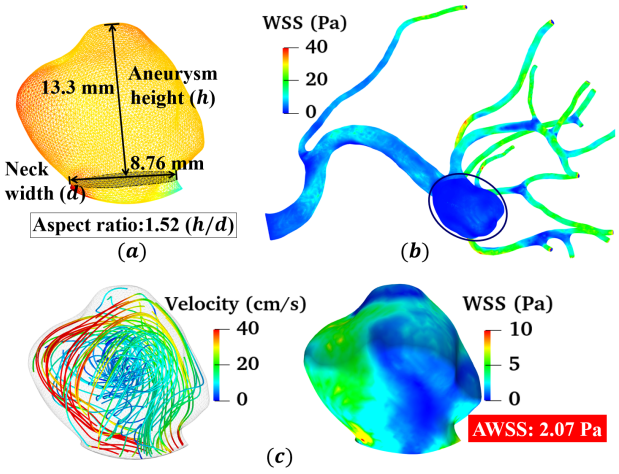

Fig. 9. Renal artery aneurysm case: the morphologic aspect ratio (a), the hemodynamic flow patterns and wall shear stress (b, c).

to assist medical experts in comprehensively diagnosing and predicting the risk of renal artery aneurysms.

C. Case study III: Localized tissue necrosis

Apart from the applications in vascular diseases, the digital twin also deepens our knowledge of kidney tissue pathologies from a hemodynamic perspective, including the interactions between the renal vasculature and the kidney tissue. For instance, localized tissue necrosis of the kidney, a condition characterized by the localized injury or death of renal tissue due to impaired blood supply or infection, can compromise kidney function and lead to further complications [25]. A comprehensive understanding of this disease will significantly improve its identification, diagnosis, and treatment. Our digital

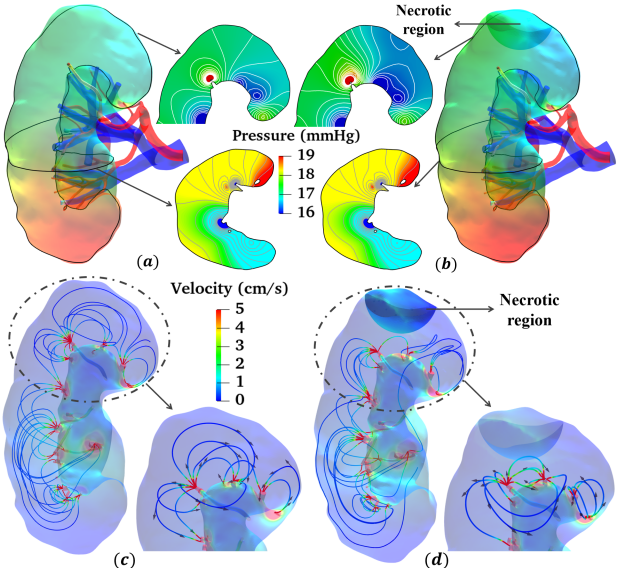

Fig. 10. Comparison of the normal tissue (left) and localized tissue necrosis (right) cases: the distribution of the pressure with local features (a, b) and the streamlines (c, d).

kidney provides global and local 3D visualizations of numerical results of the multiphysics model under different conditions of the kidney tissue. In Fig. 10, we show the numerical results of the normal kidney tissue and the localized tissue necrosis by changing the permeability. For both cases, the pressures near the necrotic region exhibit distinct distributions, with lower pressure value at the necrotic site in the localized necrosis case, while remaining similar away from the necrotic region (Fig. 10(a) and 10(b)). Such a phenomenon, with its localized effect, also appears in the streamlines and can significantly alter the local behavior of blood flow or even reduce perfusion in the necrotic region (Fig. 10(c) and 10(d)). Note that it enables users to observe differences in numerical results with respect to the location and size of the necrotic region, offering insight into their impact and enhancing understanding of the hemodynamic mechanisms.

IV. Conclusions

In this paper, we develop a digital twin of a human kidney by integrating patient-specific anatomical data, multiphysics hemodynamic modeling, and holographic visualization to advance the analysis and diagnosis of renal diseases. Within the platform, we adopt an offline-online framework for the visualization of high-fidelity numerical results, the computation of morphologic and hemodynamic indicators and the multi-expert collaborative diagnosis in real time. To understand the interactive behavior of blood flows between the renal vessels and the kidney tissue, in the offline simulation, we employ a multiphysics system coupling the unsteady incompressible Navier-Stokes equations with the unsteady Darcy equation to model the blood flows in the patient-specific renal artery, vein and kidney tissue. We discuss the applications of the

proposed digital twin to renal diseases, including renal artery stenosis, renal artery aneurysm, and localized tissue necrosis. It provides 3D visualizations of the blood velocity and pressure for these diseases. More importantly, by combining the collaborative technology and the GPU-based interactive computation of morphologic and hemodynamic factors, the digital twin enables a panel of medical experts to diagnose the risk of renal diseases in real time and consult online.

REFERENCES

[1] S. C. Textor and L. O. Lerman, "Paradigm shifts in atherosclerotic renovascular disease: where are we now?" *Journal of the American Society of Nephrology*, vol. 26, no. 9, pp. 2074–2080, 2015.

[2] C. J. White, "Catheter-based therapy for atherosclerotic renal artery stenosis," *Circulation*, vol. 113, no. 11, pp. 1464–1473, 2006.

[3] R. Subramanian, C. J. White, K. Rosenfield, R. Bashir, Y. Almagor, D. Meerkin, and E. Shalman, "Renal fractional flow reserve: a hemodynamic evaluation of moderate renal artery stenoses," *Catheterization and cardiovascular interventions*, vol. 64, no. 4, pp. 480–486, 2005.

[4] F. Tao, H. Zhang, A. Liu, and A. Y. Nee, "Digital twin in industry: State-of-the-art," *IEEE Transactions on industrial informatics*, vol. 15, no. 4, pp. 2405–2415, 2018.

[5] S. Liu, J. Bao, Y. Lu, J. Li, S. Lu, and X. Sun, "Digital twin modeling method based on biomimicry for machining aerospace components," *Journal of manufacturing systems*, vol. 58, pp. 180–195, 2021.

[6] A. McClellan, J. Lorenzetti, M. Pavone, and C. Farhat, "A physics-based digital twin for model predictive control of autonomous unmanned aerial vehicle landing," *Philosophical Transactions of the Royal Society A*, vol. 380, no. 2229, p. 20210204, 2022.

[7] I. Voigt, H. Inojosa, A. Dillenseger, R. Haase, K. Akgün, and T. Ziemssen, "Digital twins for multiple sclerosis," *Frontiers in immunology*, vol. 12, p. 669811, 2021.

[8] J. Corral-Acero, F. Margara, M. Marciniak, C. Rodero, F. Loncaric, Y. Feng, A. Gilbert, J. F. Fernandes, H. A. Bukhari, A. Wajdan *et al.*, "The 'digital twin' to enable the vision of precision cardiology," *European heart journal*, vol. 41, no. 48, pp. 4556–4564, 2020.

[9] F. Servin, J. A. Collins, J. S. Heiselman, K. C. Frederick-Dyer, V. B. Planz, S. K. Geevarghese, D. B. Brown, W. R. Jarnagin, and M. I. Miga, "Simulation of image-guided microwave ablation therapy using a digital twin computational model," *IEEE Open Journal of Engineering in Medicine and Biology*, vol. 5, pp. 107–124, 2023.

[10] Y. Gong, F. Qi, J.-Y. Wang, Y. Liu, T. Ma, Z. Cheng, Y. Jiang, R. Chen, X. Wang, L. Luo *et al.*, "An interactive platform for a high performance digital twin of a human heart," in *2023 IEEE International Conference on Metaverse Computing, Networking and Applications (MetaCom)*. IEEE, 2023, pp. 193–200.

[11] F. Qi, Y. Liu, Y. Gong, J.-Y. Wang, J. Zhou, R. Chen, R.-S. Huang, X. Wang, L. Luo, and X.-C. Cai, "Mixed reality visualization and interactive hemodynamic computation of the human brain," in *2024 IEEE International Conference on Metaverse Computing, Networking, and Applications (MetaCom)*. IEEE, 2024, pp. 17–24.

[12] Y. Zhang, G. Qin, B. Aguilar, N. Rappaport, J. T. Yurkovich, L. Pflieger, S. Huang, L. Hood, and I. Shmulevich, "A framework towards digital twins for type 2 diabetes," *Frontiers in Digital Health*, vol. 6, p. 1336050, 2024.

[13] N. Sasikaladevi and A. Revathi, "Digital twin of renal system with CT-radiography for the early diagnosis of chronic kidney diseases," *Biomedical Signal Processing and Control*, vol. 88, p. 105632, 2024.

[14] A. Mikelic and W. Jäger, "On the interface boundary condition of Beavers, Joseph, and Saffman," *SIAM Journal on Applied Mathematics*, vol. 60, no. 4, pp. 1111–1127, 2000.

[15] J.-Y. Wang, Y. Gong, J. Zhou, F. Qi, Y. Liu, Z. Cheng, R. Chen, X. Wang, L. Luo, and X.-C. Cai, "A collaborative mixed reality platform for the planning of vascular surgery," in *2024 IEEE International Conference on Metaverse Computing, Networking, and Applications (MetaCom)*. IEEE, 2024, pp. 9–16.

[16] S. K. Stoter, P. Müller, L. Cicalese, M. Tuveri, D. Schillinger, and T. J. Hughes, "A diffuse interface method for the Navier–Stokes/Darcy equations: Perfusion profile for a patient-specific human liver based on MRI scans," *Computer Methods in Applied Mechanics and Engineering*, vol. 321, pp. 70–102, 2017.

[17] E. Rohan, V. Lukeš, and A. Jonášová, "Modeling of the contrast-enhanced perfusion test in liver based on the multi-compartment flow in porous media," *Journal of mathematical biology*, vol. 77, no. 2, pp. 421–454, 2018.

[18] S. Di Gregorio, M. Fedele, G. Pontone, A. F. Corno, P. Zunino, C. Vergara, and A. Quarteroni, "A computational model applied to myocardial perfusion in the human heart: from large coronaries to microvasculature," *Journal of Computational Physics*, vol. 424, p. 109836, 2021.

[19] D. E. Keyes, L. C. McInnes, C. Woodward, W. Gropp, E. Myra, M. Pernice, J. Bell, J. Brown, A. Clo, J. Connors *et al.*, "Multiphysics simulations: Challenges and opportunities," *The International Journal of High Performance Computing Applications*, vol. 27, no. 1, pp. 4–83, 2013.

[20] Y. Liu, F. Qi, and X.-C. Cai, "An aneurysm-specific preconditioning technique for the acceleration of Newton-Krylov method with application in the simulation of blood flows," *International Journal for Numerical Methods in Biomedical Engineering*, vol. 39, no. 12, p. e3771, 2023.

[21] R. Chen, B. Wu, Z. Cheng, W.-S. Shiu, J. Liu, L. Liu, Y. Wang, X. Wang, and X.-C. Cai, "A parallel non-nested two-level domain decomposition method for simulating blood flows in cerebral artery of stroke patient," *International Journal for Numerical Methods in Biomedical Engineering*, vol. 36, no. 11, p. e3392, 2020.

[22] S. Qin, R. Chen, B. Wu, and X.-C. Cai, "A highly parallel fully implicit domain decomposition method for the simulation of the hemodynamics of a patient-specific artery at the full-body scale," *Journal of Computational Physics*, vol. 472, p. 111730, 2023.

[23] B. R. Weber and R. S. Dieter, "Renal artery stenosis: epidemiology and treatment," *International Journal of Nephrology and Renovascular Disease*, pp. 169–181, 2014.

[24] D. M. Coleman and J. C. Stanley, "Renal artery aneurysms," *Journal of vascular surgery*, vol. 62, no. 3, pp. 779–785, 2015.

[25] A. Pefanis, F. L. Ierino, J. M. Murphy, and P. J. Cowan, "Regulated necrosis in kidney ischemia-reperfusion injury," *Kidney international*, vol. 96, no. 2, pp. 291–301, 2019.

[26] X.-C. Cai, W. D. Gropp, D. E. Keyes, and M. D. Tidriri, "Newton-Krylov-Schwarz methods in CFD," in *Numerical methods for the Navier-Stokes equations: Proceedings of the International Workshop Held at Heidelberg, October 25–28, 1993*. Springer, 1994, pp. 17–30.

[27] J. E. Dennis Jr and R. B. Schnabel, *Numerical Methods for Unconstrained Optimization and Nonlinear Equations*. SIAM, 1996.

[28] Y. Liu, F. Qi, and X.-C. Cai, "A one-dimensional coarse preconditioner for three-dimensional unsteady incompressible Navier–Stokes flows in patient-specific arteries," *SIAM Journal on Scientific Computing*, vol. 46, no. 2, pp. S1–S23, 2024.

[29] Y. Liu and X.-C. Cai, "Two-level additive Schwarz methods for three-dimensional unsteady Stokes flows in patient-specific arteries with parameterized one-dimensional central-line coarse preconditioner," *J. Comput. Phys.*, p. 112290, 2023.

[30] M. Shojima, M. Oshima, K. Takagi, R. Torii, M. Hayakawa, K. Katada, A. Morita, and T. Kirino, "Magnitude and role of wall shear stress on cerebral aneurysm: computational fluid dynamic study of 20 middle cerebral artery aneurysms," *Stroke*, vol. 35, no. 11, pp. 2500–2505, 2004.

[31] R. C. Mathew, M. Gottbrecht, and M. Salerno, "CT-FFR to guide coronary angiography and intervention," *Interventional cardiology clinics*, vol. 7, no. 3, p. 345, 2018.

[32] A. Zhu, P. Connolly, and A. A. Hakimi, "Endovascular management of a large renal artery aneurysm: a case report and review of the literature," *BMC urology*, vol. 21, pp. 1–8, 2021.

[33] H. Ujiie, Y. Tamano, K. Sasaki, and T. Hori, "Is the aspect ratio a reliable index for predicting the rupture of a saccular aneurysm?" *Neurosurgery*, vol. 48, no. 3, pp. 495–503, 2001.

[34] B. A. Zambrano, H. Gharahi, C. Lim, F. A. Jaberi, J. Choi, W. Lee, and S. Baek, "Association of intraluminal thrombus, hemodynamic forces, and abdominal aortic aneurysm expansion using longitudinal CT images," *Annals of biomedical engineering*, vol. 44, pp. 1502–1514, 2016.